Neurosci. Bull. January, 2020, 36(1):11–24
https://doi.org/10.1007/s12264-019-00413-5

www.neurosci.cn
www.springer.com/12264

ORIGINAL ARTICLE

SCN9A Epileptic Encephalopathy Mutations Display a Gain-of-function Phenotype and Distinct Sensitivity to Oxcarbazepine

Shuzhang Zhang[1] · Zhiping Zhang[1] · Yuan Shen[2] · Yudan Zhu[2] · Kun Du[3] · Jingkang Guo[1] · Yonghua Ji[1,4] · Jie Tao[2,5]

Received: 12 December 2018 / Accepted: 12 April 2019 / Published online: 1 August 2019

Abstract Genetic mutants of voltage-gated sodium channels (VGSCs) are considered to be responsible for the increasing number of epilepsy syndromes. Previous research has indicated that mutations of one of the VGSC genes, *SCN9A* (Nav1.7), result in febrile seizures and Dravet syndrome in humans. Despite these recent efforts, the electrophysiological basis of *SCN9A* mutations remains unclear. Here, we performed a genetic screen of patients with febrile seizures and identified a novel missense mutation of *SCN9A* (W1150R). Electrophysiological characterization of different *SCN9A* mutants in HEK293T cells, the previously-reported N641Y and K655R variants, as well as the newly-found W1150R variant, revealed that the current density of the W1150R and N641Y variants was significantly larger than that of the wild-type (WT) channel. The time constants of recovery from fast inactivation of the N641Y and K655R variants were markedly lower than in the WT channel. The W1150R variant caused a negative shift of the G–V curve in the voltage dependence of steady-state activation. All mutants displayed persistent currents larger than the WT channel. In addition, we found that oxcarbazepine (OXC), one of the antiepileptic drugs targeting VGSCs, caused a significant shift to more negative potential for the activation and inactivation in WT and mutant channels. OXC-induced inhibition of currents was weaker in the W1150R variant than in the WT. Furthermore, with administering OXC the time constant of the N641Y variant was longer than those of the other two *SCN9A* mutants. In all, our results indicated that the point mutation W1150R resulted in a novel gain-of-function variant. These findings indicated that *SCN9A* mutants contribute to an increase in seizure, and show distinct sensitivity to OXC.

Keywords Voltage-gated sodium channel · *SCN9A* · Epilepsy · Electrophysiological function · Oxcarbazepine · Sensitivity

✉ Yonghua Ji
yhji@staff.shu.edu.cn

✉ Jie Tao
jietao_putuo@foxmail.com

[1] Institute of Biomembrane and Biopharmaceutics, Shanghai University, Shanghai 200444, China

[2] Central Laboratory and Department of Neurology, Putuo Hospital, Shanghai University of Traditional Chinese Medicine, Shanghai 200062, China

[3] Department of Clinical Laboratory, Xin Hua Hospital Affiliated to Shanghai Jiao Tong University School of Medicine, Shanghai 202150, China

[4] Xinhua Translational Institute for Cancer Pain, Xinhua Hospital Chongming Branch, Shanghai 202150, China

[5] Putuo Clinical Medical School, Anhui Medical University, Shanghai 200062, China

Introduction

The voltage-gated sodium channel (VGSC) plays a notable role in the generation and propagation of the action potentials in neurons [1]. It has been reported that VGSCs are genetically mutated in epileptic patients as well as animal models [2–5]. The VGSC subtype Nav1.7 is encoded by *SCN9A,* which is well known to be involved in the generation, development, and maintenance of pain responses [6, 7]. Nav1.7 is preferentially expressed in the peripheral nervous system [8–10] and dynamically expressed in the central nervous system, including the cerebral cortex and hippocampus [11]. Furthermore, it has

been determined that the gain-of-function mutants of *SCN9A* are involved in neuropathic pain, such as in inherited erythromelalgia, paroxysmal extreme pain disorder, and fibrotic neuropathy, whereas the loss-of-function mutants of *SCN9A* can lead to an indifference to pain [12–14]. One noteworthy finding showed *SCN9A* mutants in 21 individuals in a family suffering from febrile seizures [15]. A missense mutation of *SCN9A* (N641Y), a conserved amino-acid residue located at the intracellular loop between domains I and II of the VGSC protein, was detected in a pedigree with febrile seizures and regarded as a gain-of-function mutation. Mice carrying the *SCN9A*-N641Y mutation are more susceptible to clonic and tonic seizures induced by electrical stimulation [16]. When *SCN9A* was sequenced in 92 unrelated patients with childhood seizures occurring during febrile illness, an associated missense mutation (K655R) was found [17]. In addition, in an analysis of a cohort of 109 patients with Dravet syndrome, nine were identified with eight different *SCN9A* mutations, including K655R [16]. Collectively, these data confirm that *SCN9A* missense mutations are disease-causing for febrile seizures and Dravet syndrome. Interestingly, several *SCN9A* mutants either act as modifiers in the presence of stronger mutants or cause mild seizures by themselves, some of which also harbor splice site or missense mutations in *SCN1A* [17]. Interestingly, a few of the pathogenic *SCN9A* mutants with or without *SCN1A* mutations have been identified in epileptic patients [18, 19]. It is thus worthwhile to delve into the molecular mechanism by which *SCN9A* variants induce epileptic seizures.

Oxcarbazepine (OXC) is one of the novel anti-epileptic drugs used to control tonic-clonic seizures. It is generally well-tolerated and has a more predictable dose-response relationship than carbamazepine. One report indicates that OXC most likely has a greater effect than carbamazepine in reducing serum Na^+ levels, particularly at higher doses [20]. Moreover, it has been reported that OXC inhibits abnormal neuronal firing by targeting of voltage-dependent Na^+ channels, and reduces the excitatory synaptic transmission [21].

In this study, we set out to investigate the molecular mechanism of *SCN9A* in the generation of epilepsy. To do so, we performed a genetic screen of children with febrile seizures, and identified a novel *SCN9A* missense variant: W1150R. We then determined the electrophysiological characteristics of the variants W1150R, N641Y, and K655R and also tested the sensitivity of three gain-of-function *SCN9A* variants to OXC.

Materials and Methods

Mutation Screening

Genomic DNA was extracted from peripheral blood with kit (DP348, Tiangen, Beijing, China). The samples were assessed by Shanghai Biotechnology Corp., China. *SCN9A* variants were examined in children with febrile seizures by whole-exome sequencing. This study was approved by the Institutional Review Board at Putuo District Center Hospital, Shanghai (Putuo Hospital, Shanghai University of Traditional Chinese Medicine). And informed consent was given by the parent or guardian.

Site-Directed Mutagenesis of *SCN9A* (hNav1.7) Plasmids

Three individual point-mutations (N641Y, K655R, and W1150R) were constructed. Each amino-acid substitution was introduced into the pEZ-Lv206-hNav1.7 plasmid using a Hieff Mut^{TM} Site-Directed Mutagenesis Kit (11004ES10, Yeasen, Shanghai, China) according to the manufacturer's protocol. The constructs were verified by resequencing before transfection into HEK293T cells.

Homology Modelling

An alignment of the top 48 sequences most similar to *SCN9A* was conducted using PSI-BLAST (Discovery Studio 2017 R2, Neotrident, Shanghai, China). The cryo-EM structure of the electric eel Nav1.4 (PDB ID 5XSY) [22] served as the structural template to construct wild-type and W1150R homology models of hNav1.7, using the MODELER. MODELER selected the optimal model based on probability density function (PDF) or discrete optimized protein energy (DOPE) values. When the PDF of the total energy of a structural model is the same, the DOPE score, based on the atomic statistical potential energy, can be used as a basis for measuring the quality of the model.

Cell Transfection

HEK293T cells were grown in a humidified atmosphere of 5% CO_2 and 95% air at 37 °C in Dulbecco's modified Eagle's medium (Invitrogen, CA) supplemented with 10% fetal bovine serum (Invitrogen), then seeded in 24-well plates 24 h before transfection. Wild-type pEZ-Lv206-hNav1.7 plasmids or mutants were transfected into HEK293T cells together with pIRES-EGFP-hβ1 using Lipofectamine 3000 (Invitrogen) with 4 μg of plasmids and 1 μg pIRES-EGFP-hβ1 according to the manufacturer's

instructions. Electrophysiological recordings from fluorescent cells were made 48 h after transfection.

Chemicals and Solutions

OXC from Sigma (Poole, UK) was dissolved in extracellular solution containing 1‰ dimethyl sulfoxide at 120 μmol/L [23, 24].

Electrophysiological Recording

The patch clamp recordings were performed at room temperature using EPC-10USB (HEKA Elektronik, Germany). Data were acquired and analyzed using Patchmaster (HEKA Elektronik). Cells recognized by the marker genes Cherry (pEZ-Lv206-hNav1.7) and GFP (pIRES-EGFP-hβ1) were chosen for patch clamp recording. The solutions used for whole-cell voltage clamp recording were: extracellular solution (in mmol/L): 140 NaCl, 2 $CaCl_2$, 2 $MgCl_2$, 10 HEPES, and 10 D-glucose, pH 7.3 with NaOH (320 mOsm adjusted with D-glucose); and intracellular solution (in mmol/L): 140 CsF, 10 CsCl, 2 $MgCl_2$, 10 EGTA, 10 HEPES, pH 7.3 with CsOH, osmolality adjusted to 310 mOsm with D-glucose. The patch pipettes had resistances of 2 MΩ–5 MΩ when filled with pipette solution. Cells were held at − 120 mV in all experiments. When voltage errors were used with 80% series resistance compensation, this cell can be used for data statistics.

The peak currents were determined using 100-ms pulses from − 100 mV to + 75 mV in 5-mV steps from a holding potential of − 120 mV at 5-s intervals. The peak current was normalized for cell capacitance, and plotted against voltage to generate the peak current density–voltage relationship. Conductance as a function of voltage was obtained from the current–voltage relationship: $G(V) = I(V)/(V - Er_{Na})$ and fitted by the Boltzmann function: $G = I/(1 + \exp[(V - V_{1/2})/K])$ to determine the voltage midpoint ($V_{1/2}$) and slope factor (K). For steady-state inactivation, cells were held at − 140 mV and the test potential was from − 140 mV to 20 mV for 600 ms at 10-mV increments. A second pulse to − 10 mV for 50 ms was used to assess channel availability. The normalized current was plotted against voltage, and steady-state inactivation curves were also fitted with the Boltzmann equation as above to determine the voltage midpoint ($V_{1/2}$) and slope factor K. To generate fast inactivation curves, cells were stepped to inactivating potentials from − 140 mV to 20 mV for 60 ms followed by a 50-ms step to − 10 mV as the second pulse. The fast inactivation peak current was normalized by maximum current amplitude, and fitted by Boltzmann function as above to determine the voltage midpoint ($V_{1/2}$) and slope factor K. For recovery from inactivation, cells were held at − 120 mV and depolarized to a test potential of 0 mV for 50 ms to inactivate Na^+ channels. Recovery was determined at times between 2 ms and 40 ms with a test potential of − 140 mV. A 50-ms pulse to − 10 mV was subsequently applied to assess the extent of channel recovery. Peak current was normalized by maximum current amplitude and fitted with a single exponential function: $I/I_{max} = A[1 - \exp(-t/\tau_{rec})]$ to determine the time constant τ.

For experiments including the testing of OXC, electrophysiological protocols under control, drug-free conditions were obtained before bath application of OXC (120 μmol/L, 5 min).

Statistical Analysis

Data were analyzed with OriginPro 8.5 (OriginLab, CA), Excel 2016 (Microsoft, WA) and Prism 6 (GraphPad software, San Diego, CA). Data are presented as the mean ± standard error of the mean (SEM). Student's *t*-test or one-way ANOVA was used to assess the statistical significance of differences. When $P < 0.05$, differences were accepted as significant.

Results

Identification of an Identical *De Novo* Variant in *SCN9A* (hNav1. 7) from a Patient with Febrile Seizures

We identified a novel variant c3488T > C [p.(W1150R)] in a patient with febrile seizures. The patient presented at age 2 with complex focal seizures with secondary generalization. The patient's first seizure (generalized tonic-clonic seizure for 5 min) developed with fever (38.6 °C). The EEG showed high-potential spike activity, paroxysmal release, and δ frequency power enhancement. At age 3, seizures occurred 4 times with fever (38 °C–39.5 °C), the longest lasting 10 min. The patient had no pain or malnutrition. Growth and mental development were the same as his peers. His grandfather had a history of febrile seizures but there was no additional family history of epilepsy.

We determined that the location of amino-acid W1150 was in the domain II/III cytoplasmic linker of Nav1.7 (Fig. 1A). A previous study already reported that two mutants (N641Y and K655R) are located in the domain I/II cytoplasmic linker of Nav1.7 [16] (Fig. 1A). Therefore, we constructed three plasmids: *SCN9A*-N641Y, *SCN9A*-K655R, and *SCN9A*-W1150R (Fig. 1B).

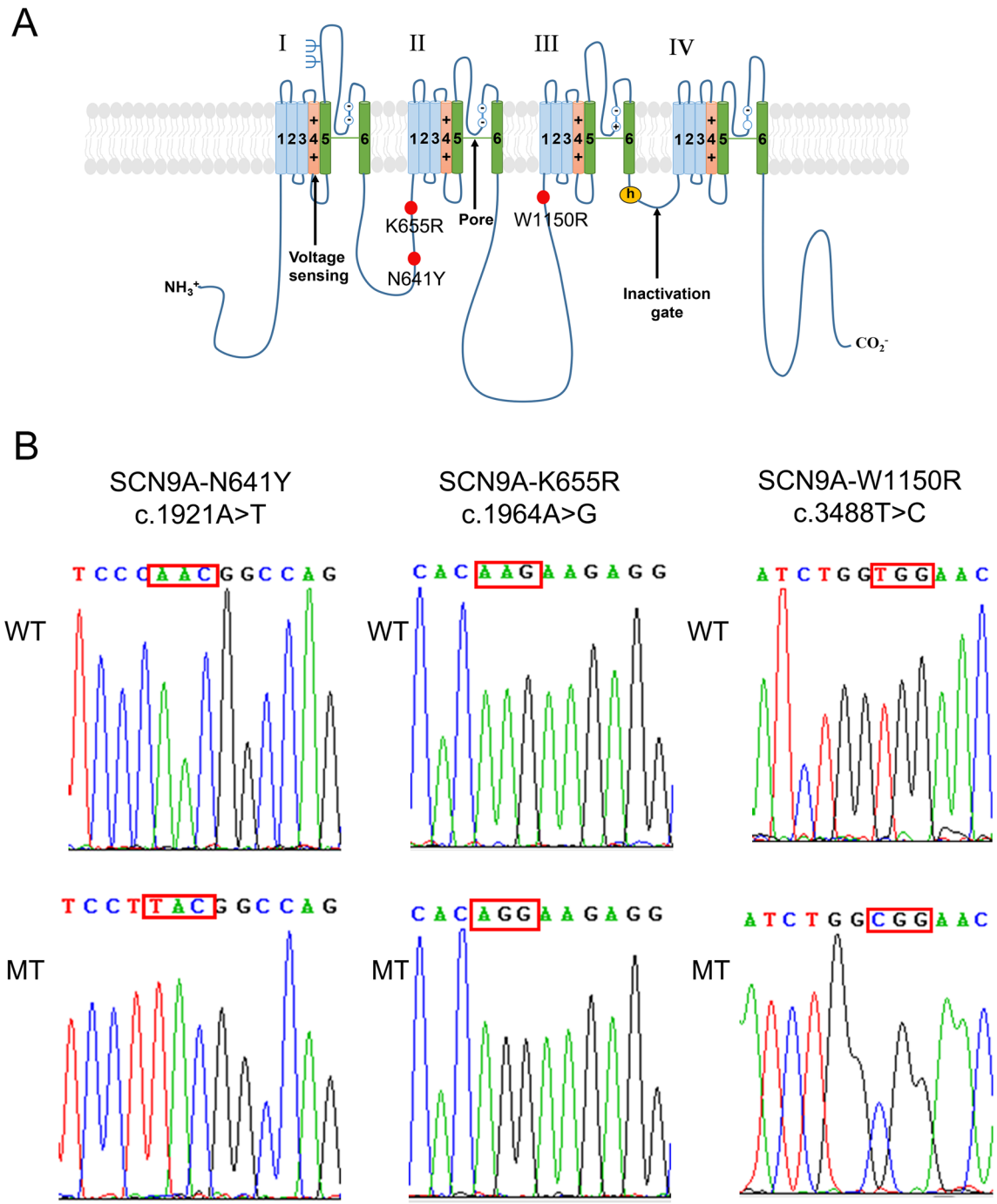

Fig. 1 Location and sequencing of the *SCN9A* variants. **A** Predicted transmembrane topology of *SCN9A* depicting the location of the variants. The S4 segments are voltage sensors and marked with plus signs. **B** DNA sequencing identified the mutations in the constructed pEZ-Lv206-hNav1.7 plasmid. The mutation sites are marked by a red squares.

Activation Properties of hNav1.7 Variants

Homology modeling revealed that the hNav1.7 mutation W1150R altered the α-helix of the S1 segment in domain III (Fig. 2). Representative currents of hNav1.7 and variants co-expressed with hβ1 subunits in HEK293T cells are illustrated in Fig. 3A. The average peak current density–voltage relationships were measured from cells transiently expressing mutants or hNav1.7 (Fig. 3B). We measured the peak current densities of the three variants and found that those of the W1150R and N641Y variants were significantly larger than that of the WT channel (WT, $-$ 109.5 $\pm$ 10.4 pA/pF, n = 11; N641Y, $-$ 183.4 $\pm$ 16.9 pA/pF, n = 16, $P < 0.01$; W1150R, $-$ 159.1 $\pm$ 15.1 pA/pF,

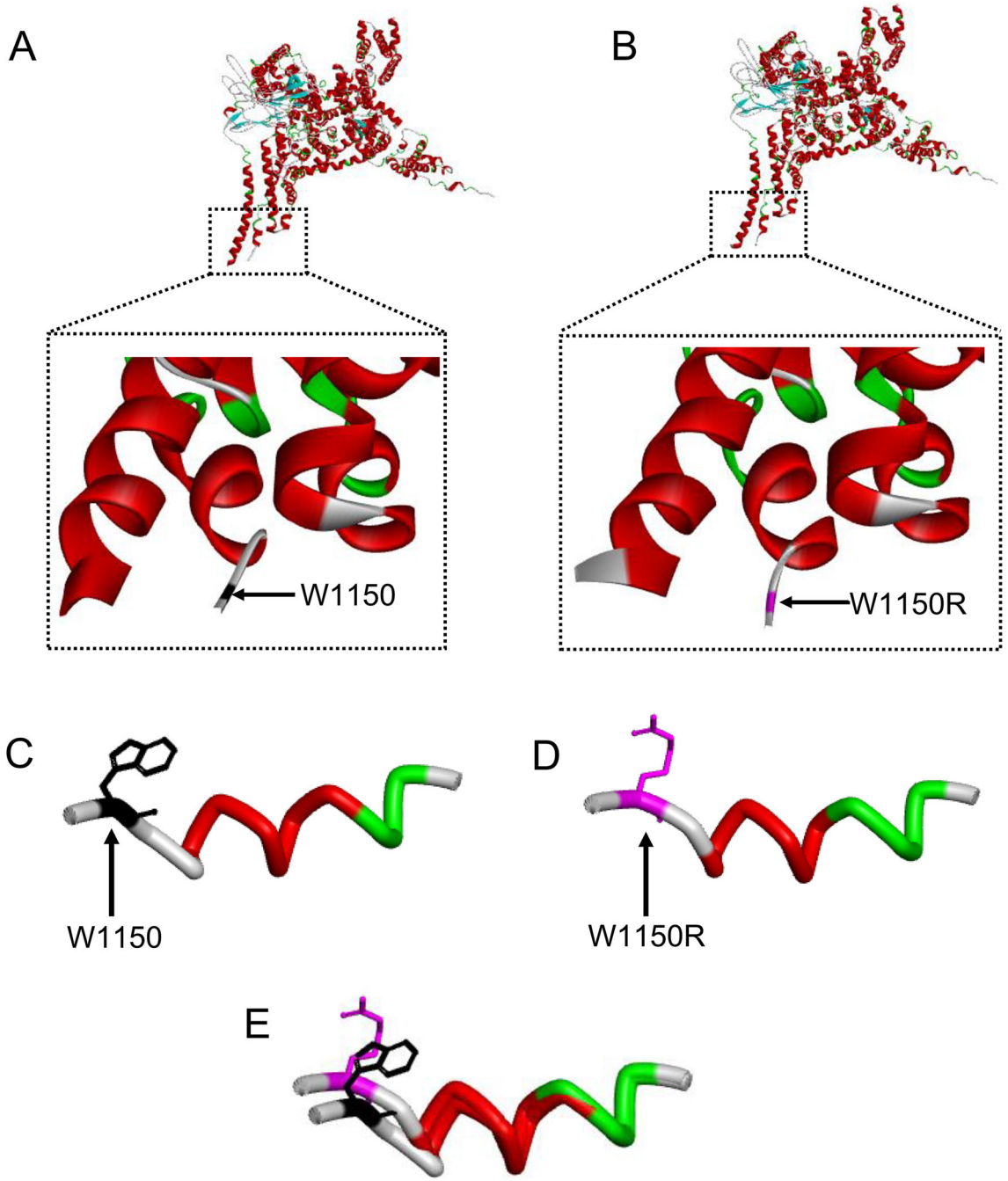

Fig. 2 W1150R mutation affects the α-helix of the S1 segment in domain III. **A, B** Schematics of the backbone structure of the wild-type and mutated domains. **C–E** Stick diagrams of the S1 segment of domain III of the wild-type and W1150R mutant. Black, W1150; magenta, W1150R.

$n = 8$, $P < 0.05$; Table 1). However, the current density of the K655R variant did not significantly differ from WT channels (K655R, − 134.4 ± 12.2 pA/pF, $n = 10$; Table 1). Using statistical analysis, we also found a large hyperpolarizing shift of the *G–V* curve for the voltage-dependence of steady-state activation that occurred in the W1150R variant ($V_{1/2}$ by − 4.3 mV; $n = 12$, $P < 0.05$; Fig. 3C, D, Table 1). On the contrary, the N641Y and K655R variants presented a marked depolarizing shift of the *G–V* curve (Fig. 3C, D). The $V_{1/2}$ values for the N641Y and K655R variants were − 15.0 ± 0.6 mV and − 16.0 ± 1.8 mV, respectively (Table 1). There was no difference in the slope factor (*K*) for any of the mutants when compared with the control group (Fig. 3E, Table 1). The transition from the open to the inactivated state was delayed in the W1150R variant at depolarizing voltages ranging + 20 mV and + 70 mV (Fig. 3F), but in the K655R variant the transition was delayed between + 20 mV and + 40 mV. As for the

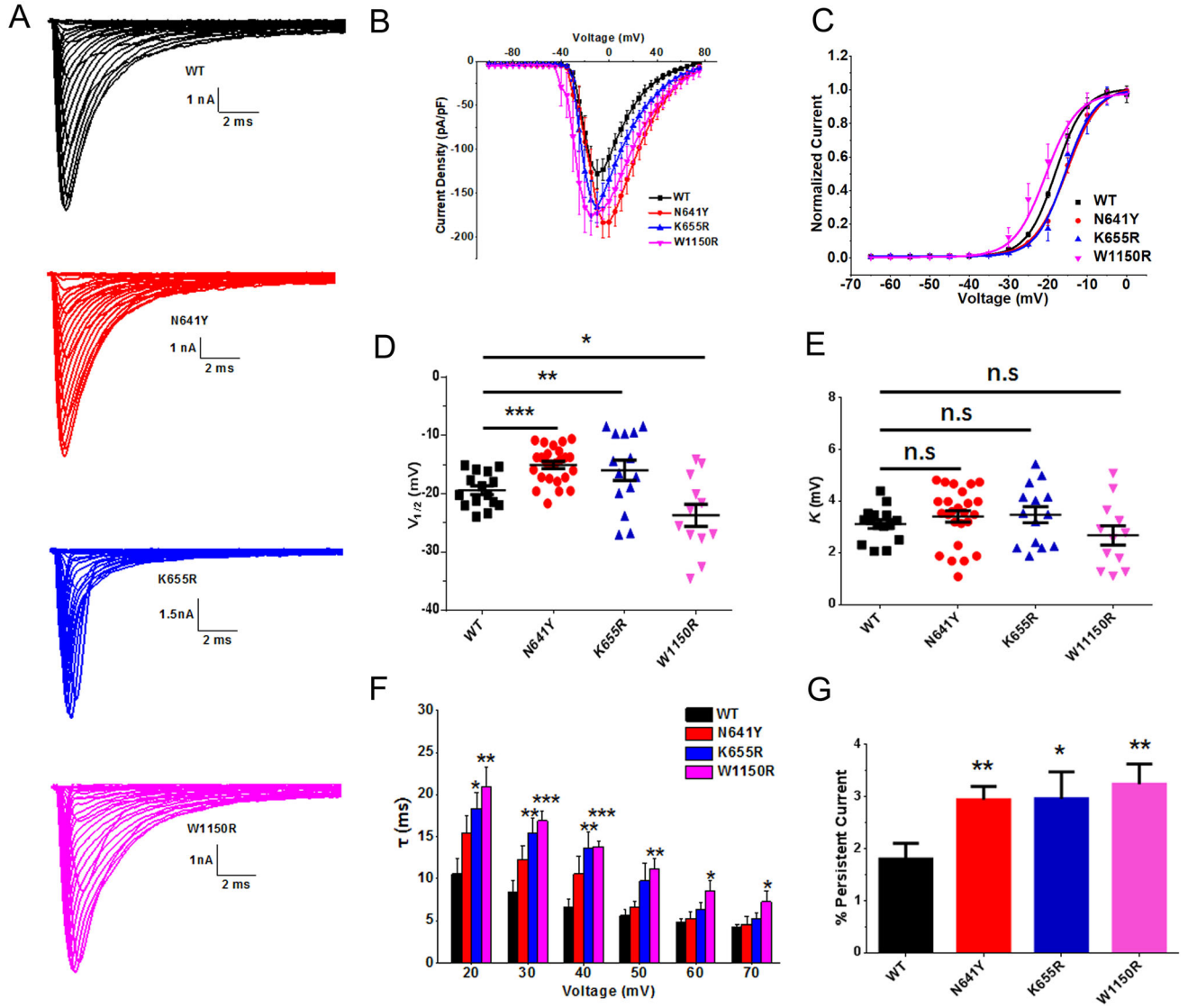

Fig. 3 Steady-state activation of *SCN9A* variants and hNav1.7. **A** Average Na^+ current traces recorded from HEK293T cells co-expressing pEZ-Lv206-hNav1.7 and pIRES-EGFP-hβ1 plasmids. **B** Average current density–voltage relationship. Peak currents were normalized to cell capacitance. **C** Voltage-dependence of steady-state activation of WT and variants. Curves are Boltzmann fits of the data. **D** Scatter plots of voltage at half-maximal steady-state activation ($V_{1/2}$) for WT and variants. **E** Scatter plots of the slope factor of activation (K). **F** Average fast time constants (τ) from single exponential fits to macroscopic current decays as a function of voltage. **G** Magnitude of persistent current as a percentage of the peak current at − 10 mV. Data are the mean ± SEM. $^*P < 0.05$, $^{**}P < 0.01$, $^{***}P < 0.001$. Black, WT; red, N641Y; blue, K655R; magenta, W1150R.

N641Y variant, the open time was unchanged. The persistent current generated by the three variants was greater than that of the WT channel, measured as a percentage of the peak current (N641Y = 2.9% ± 0.2%, $n = 16$, $P < 0.01$; K665R = 3.0% ± 0.5%, $n = 9$, $P < 0.05$; W1150R = 3.2% ± 0.4%, $n = 13$, $P < 0.01$; WT = 1.8% ± 0.3%, $n = 15$; Fig. 3G).

Characterization of the Inactivation of hNav1.7 Variants

To assess the voltage-dependence of steady-state inactivation and fast inactivation, cells expressing the WT and variants were tested. Compared to WT channels, there was no significant difference in any of the mutants regarding the half-maximal voltage-dependence of steady-state inactivation (WT: $V_{1/2} = -67.0 \pm 0.5$ mV, $n = 16$; N641Y: $V_{1/2} = -64.3 \pm 1.3$ mV, $n = 20$; K655R: $V_{1/2} = -66.1 \pm 0.8$ mV, $n = 18$; W1150R: $V_{1/2}$ =

Table 1 Biophysical properties of mutant and WT channels.

	Steady-state activation			Steady-state inactivation			Fast inactivation			Recovery from fast inactivation		Current density (0 mV)	
	$V_{1/2}$ (mV)	K	n	$V_{1/2}$ (mV)	K	n	$V_{1/2}$ (mV)	K	n	τ (ms)	n	pA/pF	n
WT	− 19.4 ± 0.8	3.1 ± 0.2	15	− 67.0 ± 0.5	5.4 ± 0.2	16	− 34.8 ± 0.7	8.2 ± 0.4	24	1.9 ± 0.2	10	− 109.5 ± 10.4	11
N641Y	− 15.0 ± 0.6***	3.4 ± 0.2	25	− 64.3 ± 1.3	6.2 ± 0.2*	20	− 33.0 ± 1.0	7.2 ± 0.4	20	1.3 ± 0.1*	8	− 183.4 ± 16.9**	16
K655R	− 16.0 ± 1.8**	3.5 ± 0.3	14	− 66.1 ± 0.8	5.2 ± 0.2	18	− 33.7 ± 1.0	8.1 ± 0.5	26	1.4 ± 0.1*	17	− 134.4 ± 12.2	10
W1150R	− 23.7 ± 1.9*	2.7 ± 0.4	12	− 65.4 ± 1.1	5.1 ± 0.2	14	− 33.5 ± 1.3	7.6 ± 0.7	17	2.1 ± 0.2	12	− 159.1 ± 15.1*	8

$V_{1/2}$, voltage midpoint activation or inactivation; K, slope factor; n, number of cells; τ, time constant.

Values represent the mean ± SEM.

*$P < 0.05$, **$P < 0.01$, ***$P < 0.001$, unpaired Student's t-test.

Table 2 Oxcarbazepine (OXC, 120 μmol/L) modulated the biophysical properties of mutant and WT channels.

	Activation			Steady inactivation			Fast inactivation			Recovery from fast inactivation	
	$V_{1/2}$ (mV)	K	n	$V_{1/2}$ (mV)	K	n	$V_{1/2}$ (mV)	K	n	τ (ms)	n
WT	− 19.5 ± 0.7	3.3 ± 0.1	8	− 66.3 ± 0.6	5.6 ± 0.3	9	− 38.0 ± 0.4	8.5 ± 0.3	7	1.7 ± 0.3	12
WT + OXC	− 23.6 ± 1.2**	3.7 ± 0.2	8	− 71.7 ± 1.5**	5.8 ± 0.2	9	− 46.1 ± 1.5***	8.8 ± 0.5	7	2.5 ± 0.2**	17
N641Y	− 17.0 ± 0.8	3.6 ± 0.4	6	− 62.7 ± 1.1	6.5 ± 0.1	14	− 37.1 ± 0.9	5.5 ± 0.3	9	1.3 ± 0.1	8
N641Y + OXC	− 24.6 ± 0.6***	3.7 ± 0.2	6	− 69.1 ± 1.4**	6.7 ± 0.4	14	− 46.4 ± 2.1***	4.9 ± 0.8	9	2.8 ± 0.3***	8
K655R	− 17.8 ± 1.8	3.5 ± 0.3	9	− 67.9 ± 0.3	5.1 ± 0.2	11	− 37.0 ± 0.9	8.1 ± 0.5	13	1.4 ± 0.1	17
K655R + OXC	− 24.3 ± 0.7*	3.6 ± 0.4	12	− 71.3 ± 0.7***	6.1 ± 0.2**	11	− 41.5 ± 1.2**	8.5 ± 0.5	13	1.8 ± 0.1**	16
W1150R	− 23.7 ± 1.9	2.8 ± 0.3	12	− 64.5 ± 0.5	5.6 ± 0.2	10	− 37.5 ± 1.3	8.9 ± 1.3	9	2.4 ± 0.2	11
W1150R + OXC	− 31.2 ± 2.5*	2.9 ± 0.4	12	− 73.1 ± 2.0***	6.1 ± 0.3	10	− 50.3 ± 2.3***	8.9 ± 1.0	9	3.2 ± 0.3*	11

$V_{1/2}$, voltage midpoint activation or inactivation; K, slope factor; n, number of cells; τ, time constant.

Values represent the mean ± SEM.

*$P < 0.05$, **$P < 0.01$, ***$P < 0.001$, unpaired Student's t-test.

− 65.4 ± 1.1 mV, n = 14; Fig. 4A, B, Table 1). Notably, only the slope factor of the N641Y variant was increased (n = 20, $P < 0.05$; Fig. 4C, Table 1). There were no statistical differences in the average fits for fast inactivation for the variants compared to the WT channels (WT: $V_{1/2}$ = − 34.8 ± 0.7 mV, K = 8.2 ± 0.4, n = 24; N641Y: $V_{1/2}$ = − 33.0 ± 1.0 mV, K = 7.2 ± 0.4, n = 20; K655R: $V_{1/2}$ = − 33.7 ± 1.0 mV, K = 8.1 ± 0.5, n = 26; W1150R: $V_{1/2}$ = − 33.5 ± 1.3 mV, K = 7.6 ± 0.7, n = 17; Fig. 4D–F, Table 1).

Recovery Properties of hNav1.7 Variants

We also examined the kinetic correlations between the recovery and inactivation of the WT and variants. The time constant of recovery from inactivation for the W1150R variant (2.1 ± 0.2 ms, n = 12) was similar to that of the

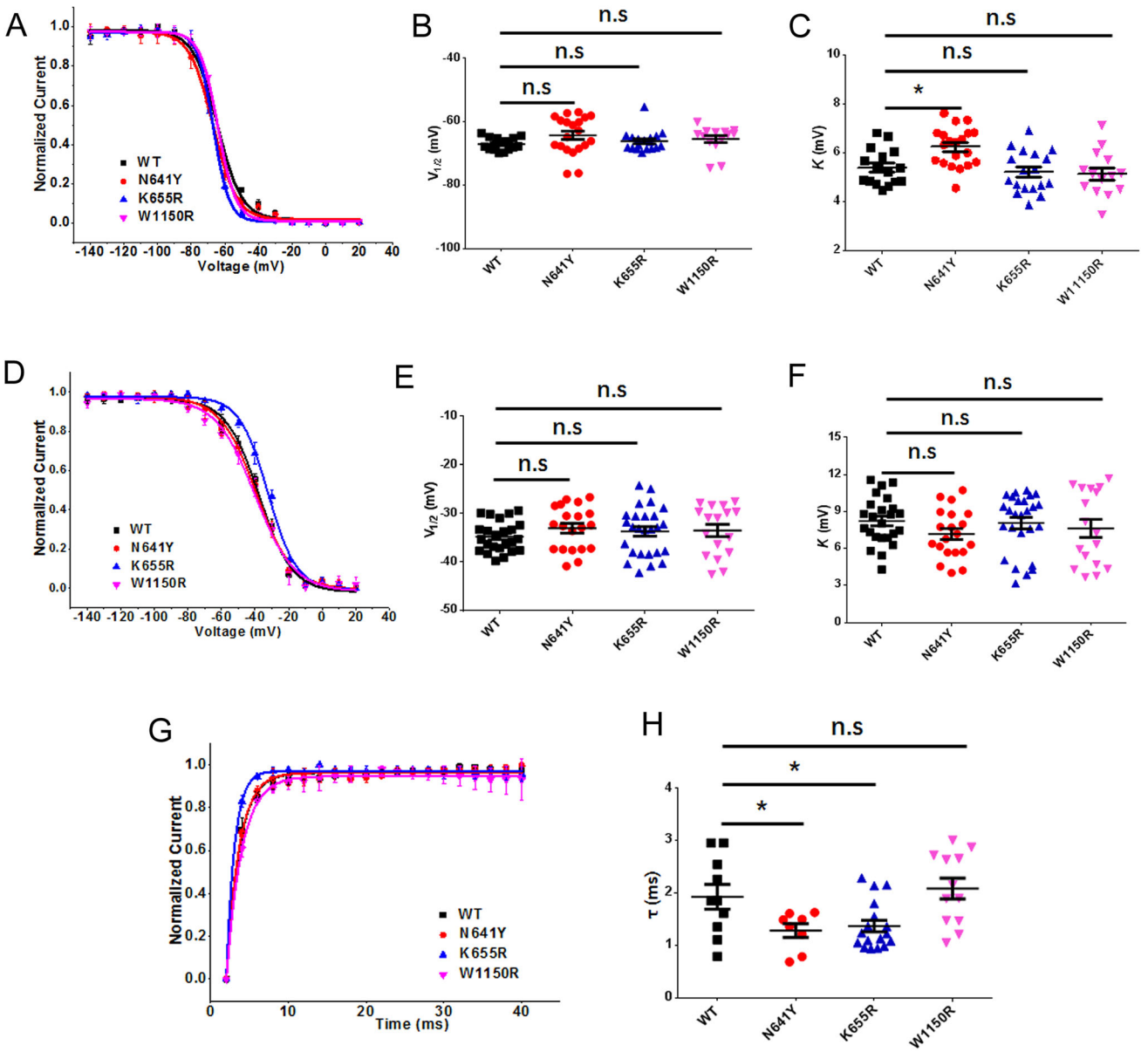

Fig. 4 Inactivation and recovery from inactivation of *SCN9A* variants and hNav1.7. **A** Voltage-dependence of steady-state inactivation of WT and variants. Curves are Boltzmann fits of the data. **B** Scatter plots of voltage at half-maximal steady-state inactivation ($V_{1/2}$) for WT and variants. **C** Scatter plots of the slope factor of steady-state inactivation (K). **D** Voltage-dependence of fast inactivation of WT and variants. Curves are Boltzmann fits. **E** Scatter plots of $V_{1/2}$ for WT and variants. **F** Scatter plots of K. **G** Voltage dependence of recovery from inactivation of WT and variants. Curves are single exponential fits of the data. **H** Scatter plots of the time constant of recovery from inactivation of WT and variants. Data are the mean ± SEM. $^*P < 0.05$, $^{**}P < 0.01$. Black, WT; red, N641Y; blue, K655R; magenta, W1150R.

WT channel (1.8 ± 0.2 ms, $n = 10$). The values for the other variants were significantly lower (N641Y: 1.3 ± 0.1 ms, $n = 8$, $P < 0.05$; K655R: 1.4 ± 0.1 ms, $n = 17$, $P < 0.05$) (Fig. 4G, H and Table 1).

Influence of Temperature on the Activation of hNav1.7 and the W1150R Variant

We determined the effects of temperature on the activation of hNav1.7 and the W1150R variant. The $V_{1/2}$ for the WT channel did not differ from the room temperature group [WT (25 °C): $V_{1/2}$ = − 19.36 ± 1.567 mV, $n = 15$; WT (38 °C): $V_{1/2}$ = − 21.42 ± 1.072 mV, $n = 19$; Fig. 5A, B]. The W1150R variant had a large hyperpolarizing shift of the *G–V* curve for the voltage-dependence of steady-state activation when the temperature was raised ($V_{1/2}$ by − 4.7 mV; $n = 7$, $P < 0.05$; Fig. 5C, D).

Effects of OXC on the Activation of hNav1.7 Variants

Representative currents from steady-state activation and those after treatment with OXC are shown in Fig. 6A. At 120 µmol/L, tonic block by OXC was significantly greater for the K655R (66.55% ± 3.4%; $n = 7$) than for the WT currents (55.23% ± 3.4%, $n = 12$, $P < 0.05$) (Fig. 6B). That of the N641Y variant (56.26% ± 3.5%, $n = 10$) was similar to the WT channel. However, the tonic block by OXC was significantly weaker for the W1150R (41.38% ± 3.2%; $n = 10$, $P < 0.01$) than for the WT currents. With the use of OXC (120 µmol/L), a tendency of negative shift for the *G–V* curve of steady-state activation occurred in the WT and variants. The difference between the half-maximal voltage values before and after OXC was significant in the N641Y variant compared to the others ($V_{1/2}$ by − 7.6 mV, $P < 0.001$) (Fig. 6C–F). The slope (K) was constant for all variants (Table 2). There was an apparent shortening in the time from the open to the inactivation state in the N641Y variant at depolarizing voltages ranging + 20 mV and + 40 mV (Fig. 7B), but this occurred in the K655R variant only at + 20 mV (Fig. 7C), while the open time for the W1150R variant was unchanged (Fig. 7D).

Effects of OXC on the Inactivation of hNav1.7 Variants

As for the steady-state inactivation, the $V_{1/2}$ of the N641Y, K665R, and W1150R variants was negatively shifted by OXC (by − 6.4 mV, $n = 14$, $P < 0.01$; by − 3.4 mV, $n = 11$, $P < 0.001$; by − 8.6 mV, $n = 10$, $P < 0.001$; respectively; Fig. 8A–D and Table 2). Treatment with OXC (120 µmol/L) also induced a hyperpolarizing shift in the voltage-dependence of the fast inactivation in the variants (N641Y $V_{1/2}$ by − 9.3 mV, $n = 9$, $P < 0.001$; K655R $V_{1/2}$ by − 4.5 mV, $n = 13$, $P < 0.01$; W1150R $V_{1/2}$

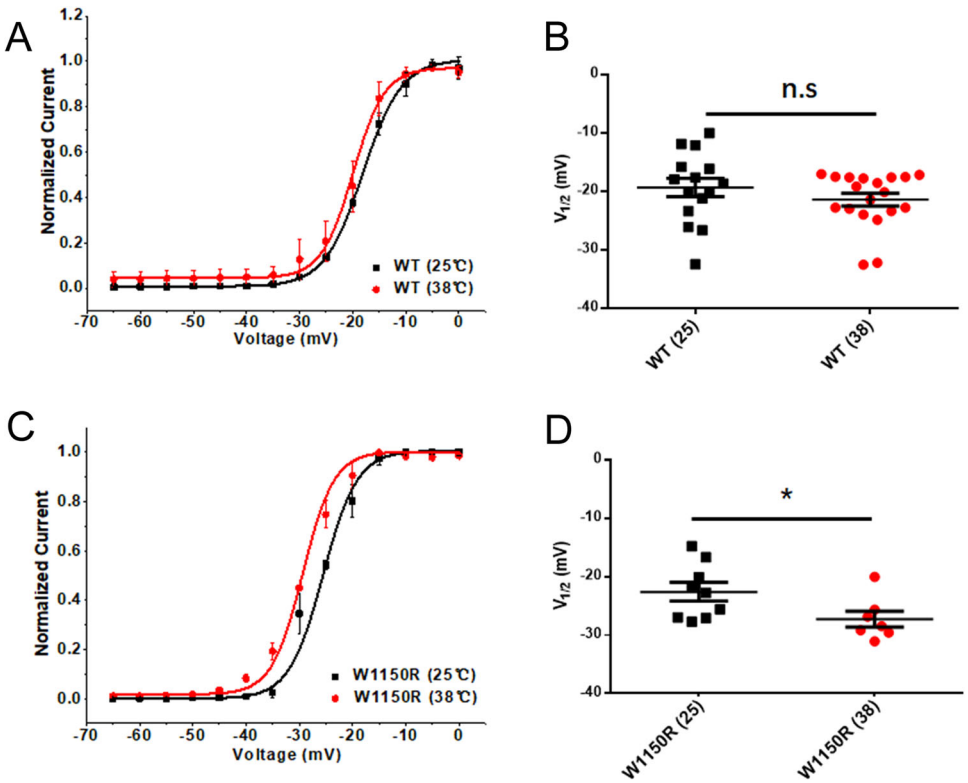

Fig. 5 Influence of temperature on the steady-state activation of hNav1.7 and the W1150R variant. **A**, **C** Voltage-dependence of steady-state activation at 25 °C and 38 °C for hNav1.7 (**A**) and the W1150R variant (**C**). Curves are Boltzmann fits. **B** Scatter plots of voltage at half-maximal steady-state activation ($V_{1/2}$) for the WT at 25 °C and 38 °C (25 °C: − 19.36 ± 1.567, $n = 15$; 38 °C: − 21.42 ± 1.072, $n = 19$). **D** Scatter plots of $V_{1/2}$ for W1150R at 25 °C and 38 °C (25 °C: − 22.57 ± 1.568, $n = 9$; 38 °C: − 27.24 ± 1.376, $n = 7$). Data are the mean ± SEM. *$P < 0.05$; black, 25 °C; red, 38 °C.

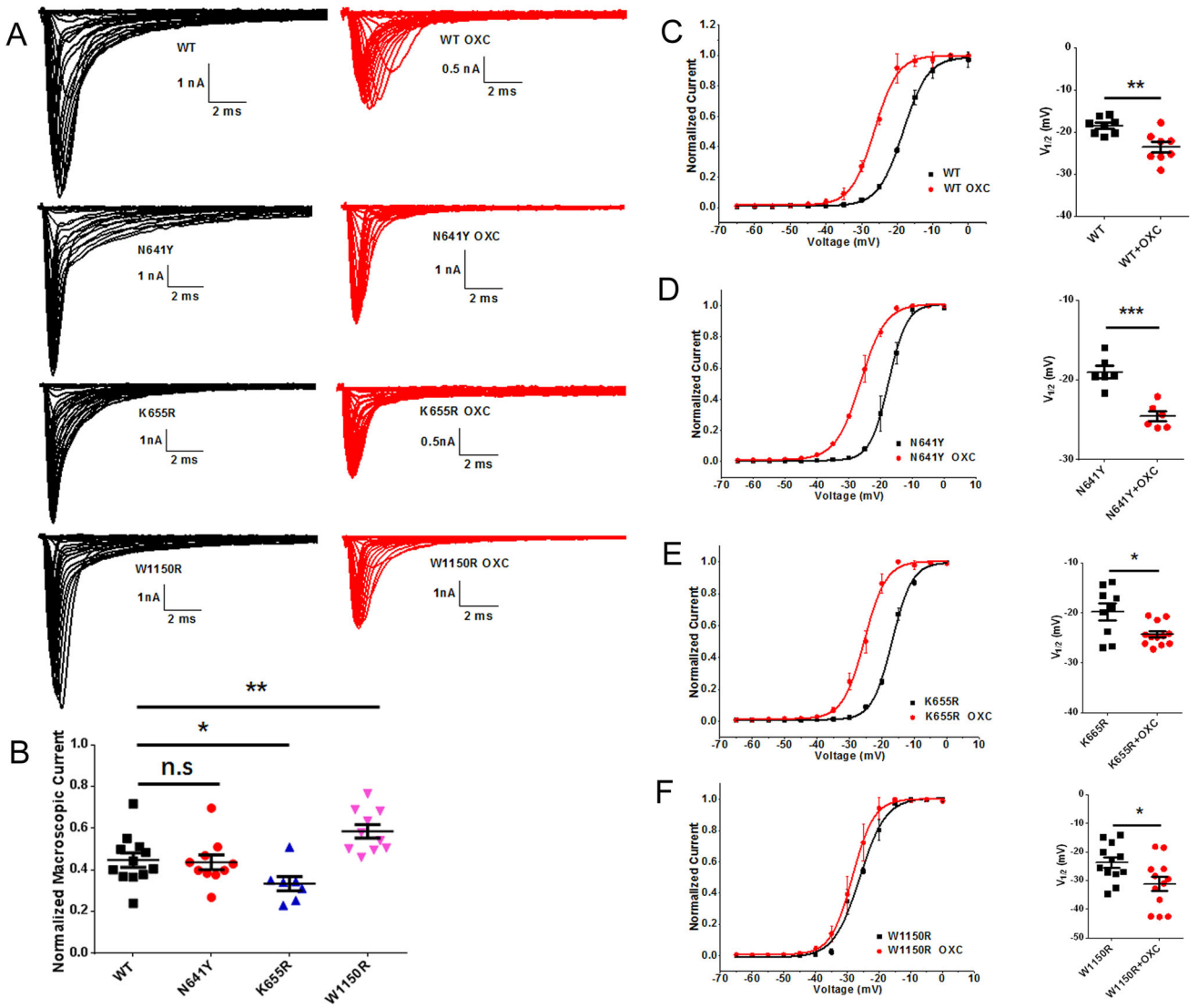

Fig. 6 Oxcarbazepine (OXC) inhibited Na^+ channel currents of hNav1.7 and *SCN9A* variants and modulates the steady-state activation. **A** Average Na^+ current traces recorded from HEK293T cells co-expressing pEZ-Lv206-hNav1.7 and pIRES-EGFP-hβ1 plasmids and treated with OXC. **B** Scatter plots showing the normalized macroscopic current amplitude remaining after blockade by OXC (120 μmol/L). **C–F** Left, shifts in the voltage-dependence of steady-state activation for WT (**C**), N641Y (**D**), K655R (**E**), and W1150R (**F**) following treatment with OXC (120 μmol/L). Curves are Boltzmann fits. Right, scatter plots of voltage at half-maximal steady-state inactivation ($V_{1/2}$). Data are the mean ± SEM. $^*P < 0.05$, $^{**}P < 0.01$, $^{***}P < 0.001$. Black, no drug treatment; red, treated with OXC.

by − 12.8 mV, $n = 9$, $P < 0.001$; Fig. F, G, H, respectively). After treatment with OXC, the voltage sensitivity (slope factor, K) was unchanged for both steady-state inactivation and fast inactivation (Table 2).

Effects of OXC on the Recovery of hNav1.7 Variants

The time constant of recovery underlying each of the hNav1.7 variants was increased in the presence of 120 μmol/L OXC, (WT by 0.8 ms, $n = 17$, $P < 0.01$; N641Y by 1.5 ms, $n = 8$, $P < 0.001$; K655R by 0.4 ms, $n = 16$, $P < 0.01$; W1150R by 0.8 ms, $n = 11$, $P < 0.05$; Fig. 9A–D and Table 2). The percentage recovery in the WT and variants decreased in the presence of 120 μmol/L OXC from 0.90 ± 0.006 for Control ($n = 8$) to 0.73 ± 0.007 for WT ($n = 7$, $P < 0.05$), 0.69 ± 0.04 for N641Y ($n = 7$, $P < 0.0001$), 0.77 ± 0.02 for K655R ($n = 12$, $P < 0.01$), and 0.63 ± 0.06 for W1150R ($n = 8$, $P < 0.01$; Fig. 9E).

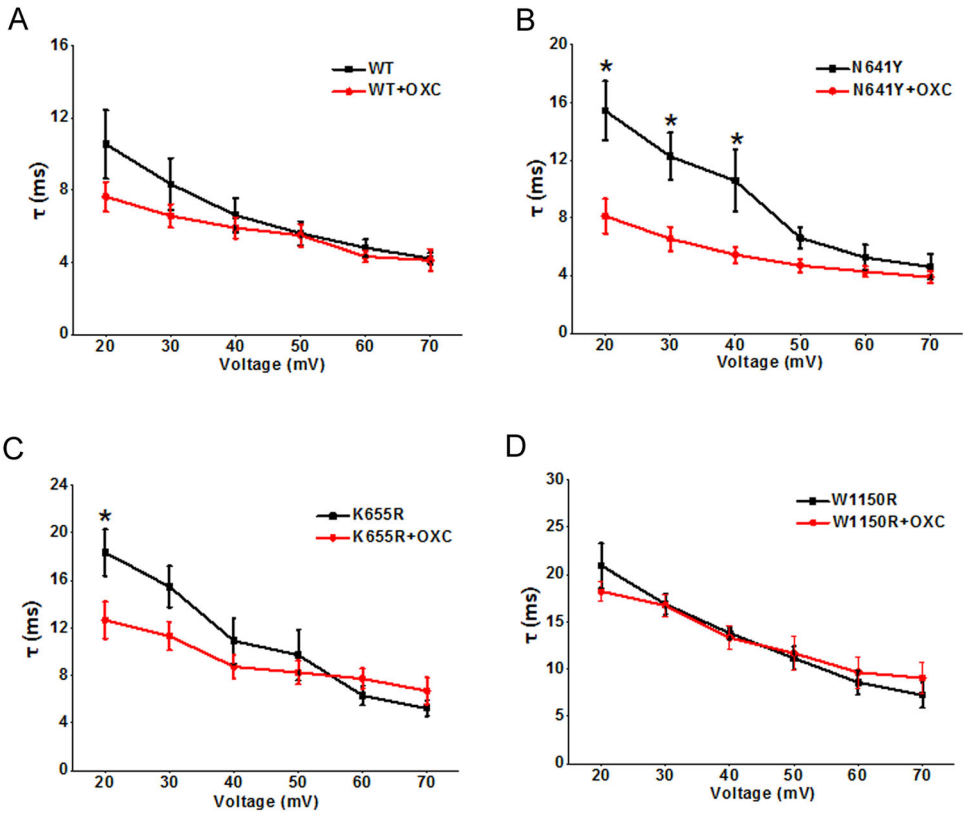

Fig. 7 Oxcarbazepine (OXC) modulates the fast time constants of hNav1.7 and *SCN9A* variants. **A**–**D** Average fast time constants of WT hNav1.7 channels (**A**), average fast time constants of p.(N641Y) mutant hNav1.7 channels (**B**), average fast time constant of p.(K655R) mutant hNav1.7 channels (**C**), and average fast time constant of p.(W1150R) mutant hNav1.7 channels (**D**) with 120 μmol/L OXC *versus* membrane potential. Data are the mean ± SEM. $^{*}P < 0.05$.

Discussion

To date, among the myriad epilepsy-associated Na^+ channel mutations described, Nav1.7 mutants have been detected in patients suffering from generalized epilepsy, temporal lobe epilepsy, febrile seizures plus, and febrile seizures [15, 16, 18, 25]. In this study, the novel *SCN9A* mutant W1150R was identified in a patient with febrile seizures. Electrophysiological characterization of W1150R suggested that the mutant is a gain-of-function variant that notably alters the kinetic properties of hNav1.7. The presence of W1150R not only leads to a significant increase in current density, but also shortens the channel activation time and markedly shifts the *G–V* curve to negative potentials. Close attention was paid to the voltage-dependent inactivation parameters of W1150R, which were constant. This implied that the window currents of the W1150R variant were increased. Increments of the window currents have been shown to reduce the action potential threshold and cause hyperexcitation [26, 27]. In addition, the W1150R variant could enhance Na^+ currents by increasing persistent currents as well as significantly prolonging the open time of hNav1.7. Several studies have supported the notion that persistent Na^+ currents also drive intrinsic neuronal excitability [28, 29]. Several epilepsy-associated Nav1.1 mutations have been found to enhance persistent currents [30–32]. Transgenic mice expressing mutant Nav1.2 channels that generate increased persistent currents display a severe epileptic phenotype [33]. Our results allow us to speculate that the generalized epilepsy induced by gain-of-function mutations in VGSC genes could be related to the facilitation of channel activation of as well as the enhancement of peak and persistent Na^+ currents.

The other hNav1.7 variants found in febrile seizure patients, N641Y and K655R, are also regarded as gain-of-function variants [16, 17]. The phenotype of these two variants in steady-state activation differs from that of W1150R. In the N641Y and K655R variants, the *G-V* curve of activation was shifted towards depolarization, and the time constant of recovery was significantly reduced. However, none of the three variants affected the inactivation. It has been shown that many mutant Na^+ channels associated with epilepsy exhibit delayed inactivation as well as increased persistent Na^+ currents [30–32]. As is generally known, a larger persistent current accentuates subthreshold depolarizations and facilitates the generation of the action potential, so we compared this property between the WT and variants, and ultimately found that the variants displayed larger persistent currents than WT channels. The above data suggested that hyperexcitability might be associated with an increased persistent current and rapid recovery of the inactivated channel to the resting

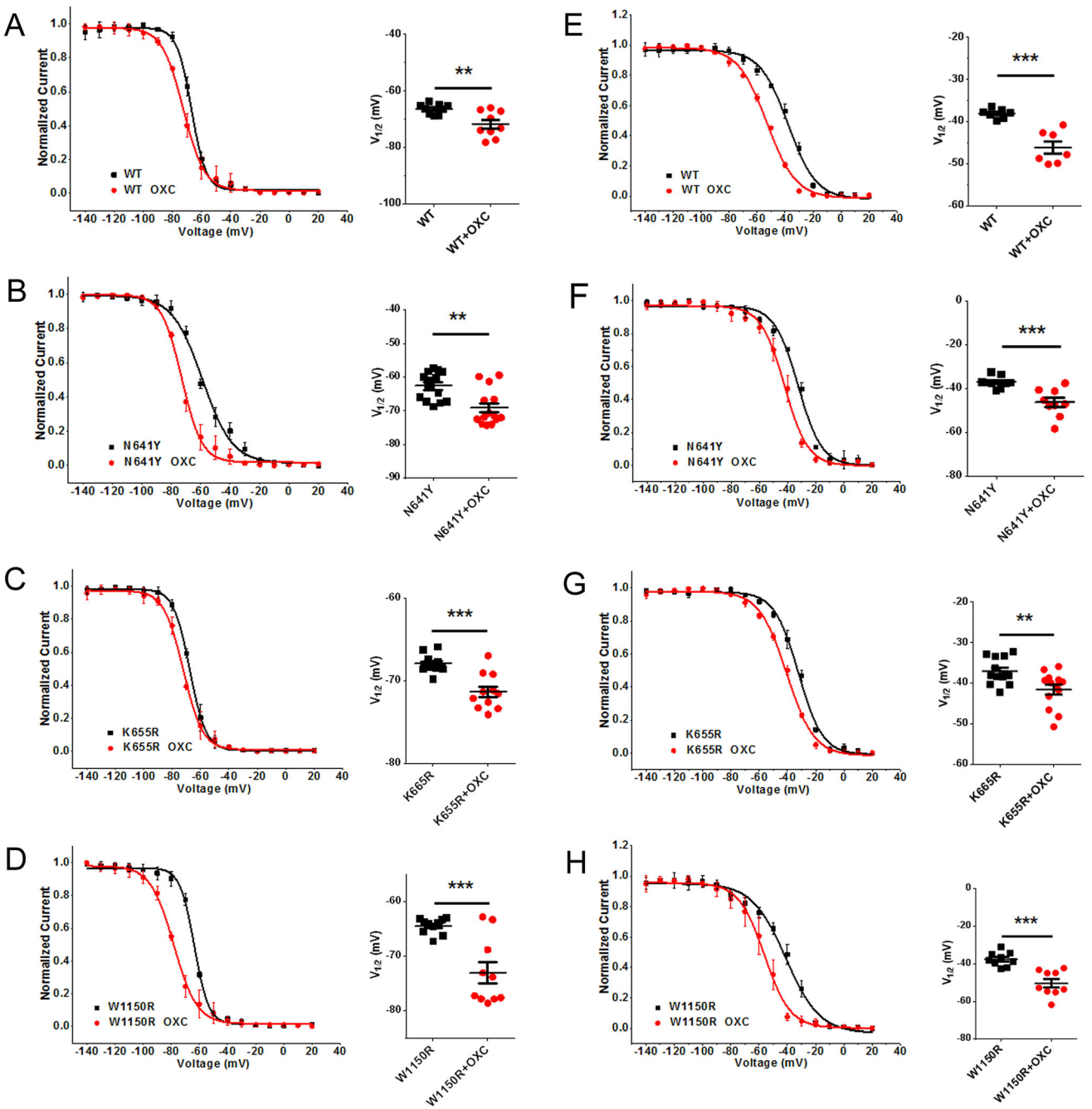

Fig. 8 Oxcarbazepine (OXC) modulated the inactivation of hNav1.7 and *SCN9A* variants. **A–D** Left, shift in the voltage-dependence of steady-state inactivation in the WT (**A**), N641Y (**B**), K655R (**C**), and W1150R (**D**) after treatment with 120 μmol/L OXC. Curves are Boltzmann fits. Right, scatter plots of voltage at half-maximal steady-state inactivation ($V_{1/2}$). **E–H** Left, shift in the voltage dependence of fast inactivation for WT (**E**), N641Y (**F**), K655R (**G**), and W1150R (**H**) after treatment with 120 μmol/L OXC. Curves are Boltzmann fits. Right, scatter plots of $V_{1/2}$. Data are the mean ± SEM. $^{**}P < 0.01$, $^{***}P < 0.001$. Black, no drug treatment; red, with OXC.

state, thereby increasing the probability that the open state of Na^+ channels was configured for longer periods.

The pharmacological data in this study revealed that treatment of both the N641Y and K655R variants with 120 μmol/L OXC resulted in a marked reduction in Na^+ currents and a shortening of the opening time. This may correspond with the capacity of OXC to inhibit abnormal neuronal firing and reduce excitatory synaptic transmission [21]. Our results implicate OXC as an effective treatment for epileptic patients with N641Y and K655R variants. However, we did find that the Na^+ currents of the W1150R variant were not significantly inhibited by OXC. At the molecular level, this could explain, in part, why patients

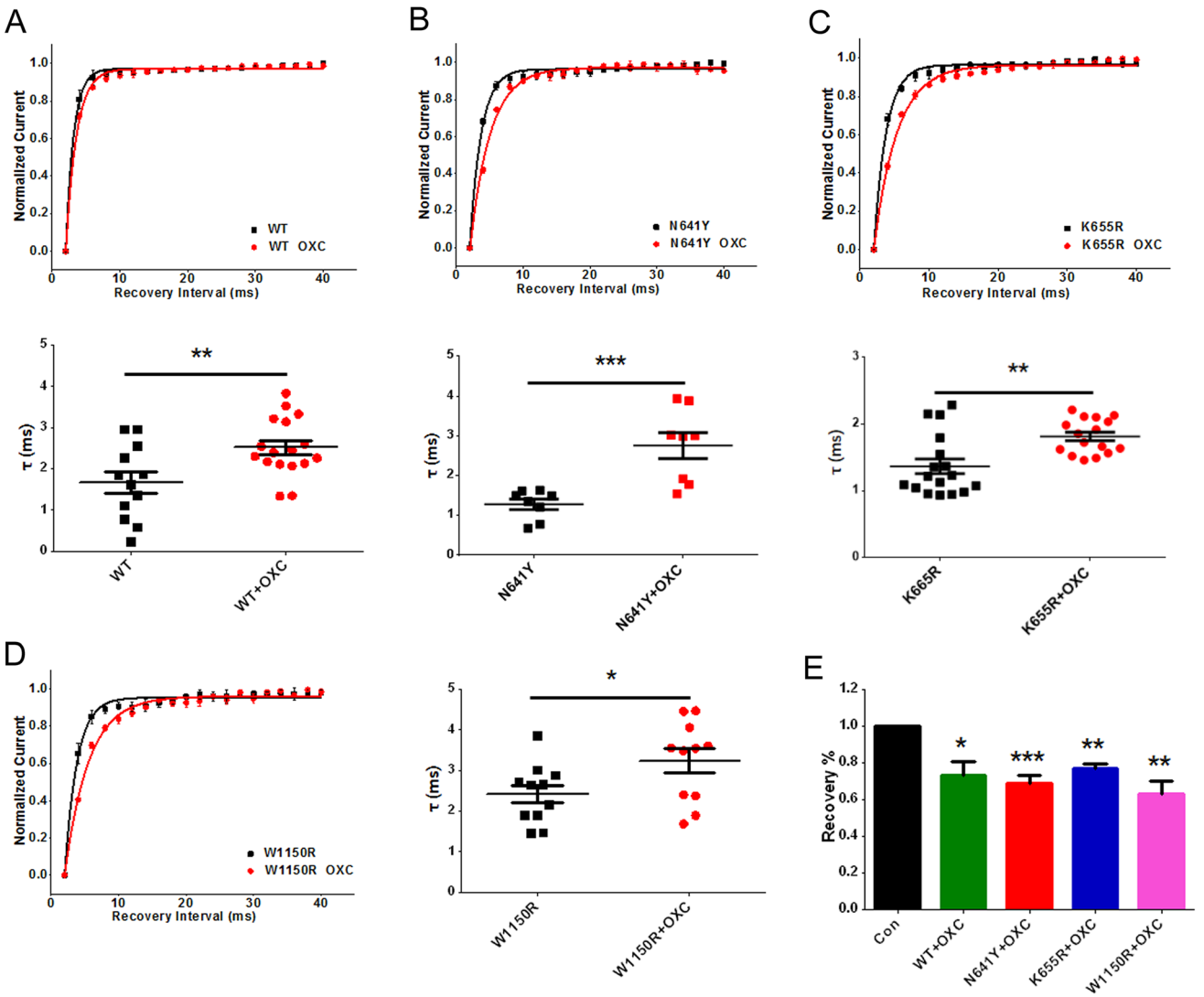

Fig. 9 Oxcarbazepine (OXC) modulated recovery from inactivation in hNav1.7 and *SCN9A* variants. **A–D** Shifts in the voltage-dependence of recovery from inactivation in the WT (**A**), N641Y (**B**), K655R (**C**), and W1150R (**D**) after treatment with 120 μmol/L OXC (curves are single exponential fits) and scatter plots of the time constant of recovery from inactivation. **E** Percentage recovery of ion channels treated with 120 μmol/L OXC. Data are the mean ± SEM. $^{*}P < 0.05$, $^{**}P < 0.01$, $^{***}P < 0.001$.

with some Nav channel mutations are not sensitive to OXC.

In summary, we have identified a novel *SCN9A* mutant (W1150R) in a patient with febrile seizures. Examination of the gain-of-function hNav1.7 mutants, N641Y, K655R, and W1150R led us to the conclusion that two of the variants are sensitive, while the W1150R variant is insensitive to OXC.

Acknowledgements We are grateful to Prof. Ren Lai and Shilong Yang (Kunming Institute of Zoology, Chinese Academy of Sciences) for providing the pEZ-Lv206-hNav1.7 plasmid. This work was supported by the National Natural Science Foundation of China (81603410, 31571032, and 31771191), the Shanghai Municipal Commission of Health and Family Planning Foundation (20184Y0086), Innovation Program of Shanghai Municipal Education Commission (15ZZ063), the Research Project of Putuo Hospital, Shanghai University of Traditional Chinese Medicine (2016102A and 2016208A), and a Project for Capacity Promotion of Putuo District Clinical Special Disease.

Conflict of interest The authors declare that they have no conflict of interest.

References

1. Cooper DC, Chung S, Spruston N. Output-mode transitions are controlled by prolonged inactivation of sodium channels in pyramidal neurons of subiculum. PLoS Biol 2005, 3: e175.
2. Vreugdenhil M, Hoogland G, van Veelen CW, Wadman WJ. Persistent sodium current in subicular neurons isolated from patients with temporal lobe epilepsy. Eur J Neurosci 2004, 19: 2769–2778.

3. Banerjee J, Fischer CC, Wedegaertner PB. The amino acid motif L/IIxxFE defines a novel actin-binding sequence in PDZ-RhoGEF. Biochemistry 2009, 48: 8032–8043.
4. Blumenfeld H, Lampert A, Klein JP, Mission J, Chen MC, Rivera M*, et al.* Role of hippocampal sodium channel Nav1.6 in kindling epileptogenesis. Epilepsia 2009, 50: 44–55.
5. Hargus NJ, Merrick EC, Nigam A, Kalmar CL, Baheti AR, Bertram EH, 3rd*, et al.* Temporal lobe epilepsy induces intrinsic alterations in Na channel gating in layer II medial entorhinal cortex neurons. Neurobiol Dis 2011, 41: 361–376.
6. Bang S, Yoo J, Gong X, Liu D, Han Q, Luo X*, et al.* Differential inhibition of Nav1.7 and neuropathic pain by hybridoma-produced and recombinant monoclonal antibodies that target Nav1.7: differential activities of Nav1.7-targeting monoclonal antibodies. Neurosci Bull 2018, 34: 22–41.
7. Chang W, Berta T, Kim YH, Lee S, Lee SY, Ji RR. Expression and role of voltage-gated sodium channels in human dorsal root ganglion neurons with special focus on Nav1.7, species differences, and regulation by paclitaxel. Neurosci Bull 2018, 34: 4–12.
8. Toledo-Aral JJ, Moss BL, He ZJ, Koszowski AG, Whisenand T, Levinson SR*, et al.* Identification of PN1, a predominant voltage-dependent sodium channel expressed principally in peripheral neurons. Proc Natl Acad Sci USA 1997, 94: 1527–1532.
9. Rush AM, Dib-Hajj SD, Liu S, Cummins TR, Black JA, Waxman SG. A single sodium channel mutation produces hyper- or hypoexcitability in different types of neurons. Proc Natl Acad Sci USA 2006, 103: 8245–8250.
10. Ahn HS, Black JA, Zhao P, Tyrrell L, Waxman SG, Dib-Hajj SD. Nav1.7 is the predominant sodium channel in rodent olfactory sensory neurons. Mol Pain 2011, 7: 32.
11. Mechaly I, Scamps F, Chabbert C, Sans A, Valmier J. Molecular diversity of voltage-gated sodium channel alpha subunits expressed in neuronal and non-neuronal excitable cells. Neuroscience 2005, 130: 389–396.
12. Dib-Hajj SD, Cummins TR, Black JA, Waxman SG. Sodium channels in normal and pathological pain. Annu Rev Neurosci 2010, 33: 325–347.
13. Cox JJ, Reimann F, Nicholas AK, Thornton G, Roberts E, Springell K*, et al.* An SCN9A channelopathy causes congenital inability to experience pain. Nature 2006, 444: 894–898.
14. Fertleman CR, Baker MD, Parker KA, Moffatt S, Elmslie FV, Abrahamsen B*, et al.* SCN9A mutations in paroxysmal extreme pain disorder: allelic variants underlie distinct channel defects and phenotypes. Neuron 2006, 52: 767–774.
15. Peiffer A, Thompson J, Charlier C, Otterud B, Varvil T, Pappas C*, et al.* A locus for febrile seizures (FEB3) maps to chromosome 2q23-24. Ann Neurol 1999, 46: 671–678.
16. Singh NA, Pappas C, Dahle EJ, Claes LR, Pruess TH, De Jonghe P*, et al.* A role of SCN9A in human epilepsies, as a cause of febrile seizures and as a potential modifier of Dravet syndrome. PLoS Genet 2009, 5: e1000649.
17. Doty CN. SCN9A: another sodium channel excited to play a role in human epilepsies. Clin Genet 2010, 77: 326–328.
18. Cen Z, Lou Y, Guo Y, Wang J, Feng J. Q10R mutation in SCN9A gene is associated with generalized epilepsy with febrile seizures plus. Seizure 2017, 50: 186–188.
19. Yang C, Hua Y, Zhang W, Xu J, Xu L, Gao F*, et al.* Variable epilepsy phenotypes associated with heterozygous mutation in the SCN9A gene: report of two cases. Neurol Sci 2018, 39: 1113–1115.
20. Dong X, Leppik IE, White J, Rarick J. Hyponatremia from oxcarbazepine and carbamazepine. Neurology 2005, 65: 1976–1978.
21. Kwan P, Sills GJ, Brodie MJ. The mechanisms of action of commonly used antiepileptic drugs. Pharmacol Ther 2001, 90: 21–34.
22. Yan Z, Zhou Q, Wang L, Wu J, Zhao Y, Huang G*, et al.* Structure of the Nav1.4-beta1 complex from electric eel. Cell 2017, 170: 470–482.e411.
23. Lee CY, Lai HY, Chiu A, Chan SH, Hsiao LP, Lee ST. The effects of antiepileptic drugs on the growth of glioblastoma cell lines. J Neurooncol 2016, 127: 445–453.
24. Booker SA, Pires N, Cobb S, Soares-da-Silva P, Vida I. Carbamazepine and oxcarbazepine, but not eslicarbazepine, enhance excitatory synaptic transmission onto hippocampal CA1 pyramidal cells through an antagonist action at adenosine A1 receptors. Neuropharmacology 2015, 93: 103–115.
25. Scheffer IE, Wallace RH, Mulley JC, Berkovic SF. Locus for febrile seizures. Ann Neurol 2000, 47: 840–841.
26. Ellerkmann RK, Remy S, Chen J, Sochivko D, Elger CE, Urban BW*, et al.* Molecular and functional changes in voltage-dependent Na(+) channels following pilocarpine-induced status epilepticus in rat dentate granule cells. Neuroscience 2003, 119: 323–333.
27. Ketelaars SO, Gorter JA, van Vliet EA, Lopes da Silva FH, Wadman WJ. Sodium currents in isolated rat CA1 pyramidal and dentate granule neurones in the post-status epilepticus model of epilepsy. Neuroscience 2001, 105: 109–120.
28. Alzheimer C, Schwindt PC, Crill WE. Modal gating of Na^+ channels as a mechanism of persistent Na^+ current in pyramidal neurons from rat and cat sensorimotor cortex. J Neurosci 1993, 13: 660–673.
29. Baker MD, Chandra SY, Ding Y, Waxman SG, Wood JN. GTP-induced tetrodotoxin-resistant Na^+ current regulates excitability in mouse and rat small diameter sensory neurones. J Physiol 2003, 548: 373–382.
30. Holland KD, Kearney JA, Glauser TA, Buck G, Keddache M, Blankston JR*, et al.* Mutation of sodium channel SCN3A in a patient with cryptogenic pediatric partial epilepsy. Neurosci Lett 2008, 433: 65–70.
31. Kahlig KM, Rhodes TH, Pusch M, Freilinger T, Pereira-Monteiro JM, Ferrari MD*, et al.* Divergent sodium channel defects in familial hemiplegic migraine. Proc Natl Acad Sci USA 2008, 105: 9799–9804.
32. Spampanato J, Kearney JA, de Haan G, McEwen DP, Escayg A, Aradi I*, et al.* A novel epilepsy mutation in the sodium channel SCN1A identifies a cytoplasmic domain for beta subunit interaction. J Neurosci 2004, 24: 10022–10034.
33. Kearney JA, Plummer NW, Smith MR, Kapur J, Cummins TR, Waxman SG*, et al.* A gain-of-function mutation in the sodium channel gene Scn2a results in seizures and behavioral abnormalities. Neuroscience 2001, 102: 307–317.